Analysis of a Noncoherent UWB Receiver for Multichannel Signals

Paul Meissner and Klaus Witrisal
Graz University of Technology, Graz, Austria, {paul.meissner, witrisal}@tugraz.at

***Abstract*—We present a detailed analysis of a previously introduced multichannel autocorrelation receiver (MC-AcR) for multichannel ultra-wideband (UWB) signals. Performance measures are introduced and discussed to provide insight in the invertibility problem for this receiver, the capability to separate the multichannel UWB signal. The results can be used for understanding the impact of hardware imperfections and for the optimization of signal parameters.**

I. Introduction

This paper deals with the analysis of a previously introduced MC-AcR for multichannel UWB signals [1], [2], where analog hardware is used to estimate samples of the autocorrelation function (ACF) of the received signal, and digital backend processing to separate the channels of the UWB signal. The receiver combines the key advantage of a noncoherent UWB receiver – it can collect energy from all multipath components at low complexity in the analog domain – with the key advantage of a multicarrier signaling scheme – an increased data rate. The analysis concentrates on the separability of a multichannel signal with the MC-AcR. Performance measures are discussed to find optimal pulse shapes for the transmit signal, to optimize parameters of the receiver, and to evaluate the impact of hardware imperfections.

An orthogonality condition for the subchannel signals at the receiver output is shown, which leads to a linear multiple-input multiple-output (MIMO) signal model. At the transmitter, we use an orthogonal frequency division multiplexing (OFDM) signal as well as a signal consisting of pulses with correlation properties optimized with the genetic optimization algorithm (GA) [3]. The latter has the advantage of employing the full signal bandwidth for each subchannel, thus improving the fading resistance.

The transmission of information in the autocorrelation function of a signal has also been used in [4], but for a multiuser application. It is also motivated by [5], where it has been shown that the ACF of a received UWB pulse suffers much less distortion by multipath propagation than the pulse itself.

The paper is organized as follows: Section II introduces the mathematical model for the data transmission, Section III introduces performance measures, Section IV deals with the pulse shape design, Section V presents simulation results and Section VI draws conclusions.

II. Mathematical Modeling

The transmitted multichannel signal consists of N subchannels. With the binary data symbols $s_n \in \{0, 1\}$ and the subchannel pulse waveforms $w_n(t)$, this signal is expressed as

$$s(t) = \sum_{n=1}^{N} s_n w_n(t) \tag{1}$$

Inter-symbol-interference (ISI) is avoided with a zero guard interval (GI), so we just consider a single symbol. The signal $s(t)$ passes a linear multipath channel with impulse response (IR) $h(t)$ and a frontend filter $f_{rx}(t)$, which is used for filtering out-of-band noise. In the following, the filter and the channel are denoted by their combined IR $\tilde{h}(t) = h(t) * f_{rx}(t)$.

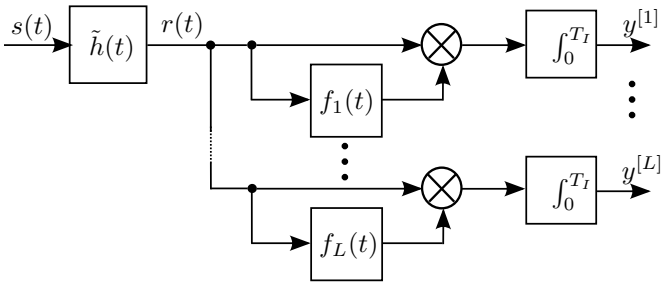

Fig. 1. Block diagram of the receiver frontend structure. The filters $f_l(t)$ will usually be pure delays, which results in a multichannel autocorrelation receiver.

The receiver frontend structure is shown in Fig. 1. It consists of L channels, in which the received signal is multiplied with a filtered version of itself. The output sample of the l-th channel is the integral of this product signal over a duration T_I

$$y^{[l]} = \int_{\tau_0}^{\tau_0+T_I} r(t)(r(t) * f_l(t))dt \tag{2}$$

where $*$ denotes convolution. The integration start offset τ_0 indicates a possibly non-ideal synchronization. Note that if the filters $f_l(t)$ are a set of ideal delays, denoted by $\{D_l\}$, the output samples $y^{[l]}$ will be samples of the autocorrelation function of the received signal.

The received signal is expressed as

$$r(t) = \sum_{n=1}^{N} s_n g_n(t) + n(t) \tag{3}$$

where $g_n(t)$ denotes the filtered UWB channel response to the n-th subchannel pulse $w_n(t)$ and $n(t)$ is a Gaussian noise process that is filtered by the receiver frontend filter.

We want to investigate the nonlinear behavior of the proposed receiver frontend structure, focussing on the influence

978-1-4244-2519-8/10/$26.00 ©2010 IEEE

of the subchannel pulse waveforms. Inserting (3) in (2) and expanding the products between all data-modulated channels as well as the noise yields the output of one AcR channel [1]

$$y^{[l]} = \sum_n s_n^2 h_{n,n}^{[l]} + \sum_n \sum_{\substack{n' \\ n' \neq n}} s_n s_{n'} h_{n,n'}^{[l]} + \nu^{[l]} \qquad (4)$$

$$\text{with} \qquad h_{n,n'}^{[l]} = \int_{\tau_0}^{\tau_0+T_I} g_n(t)(g_{n'}(t) * f_l(t))dt \qquad (5)$$

The last term in (4) corresponds to all the signal-by-noise and noise-by-noise crossterms, while the double sum corresponds to crossterms between data-modulated subchannels with unequal channel indices. Next we build an $(L \times 1)$ vector $\mathbf{y}$ of all frontend output samples, an $(N \times 1)$ vector $\mathbf{s}$ containing all data bits and a vector of all noise contributions $\boldsymbol{\nu}$. We arrange the $h_{n,n}^{[l]}$ in the l-th row and n-th column of the $(L \times N)$ *channel matrix* $\mathbf{H}$ and the $h_{n,n'}^{[l]}$ with unequal indices in the $(L \times N(N-1))$ *interference matrix* $\mathbf{G}$. Hence the structure of $\mathbf{H}$ is such that the contributions of one transmit signal subchannel are contained in one of its columns

$$\mathbf{H} = \begin{bmatrix} h_{1,1}^{[1]} & h_{2,2}^{[1]} & \cdots & h_{N,N}^{[1]} \\ h_{1,1}^{[2]} & h_{2,2}^{[2]} & \cdots & h_{N,N}^{[2]} \\ \vdots & \vdots & \ddots & \vdots \\ h_{1,1}^{[L]} & h_{2,2}^{[L]} & \cdots & h_{N,N}^{[L]} \end{bmatrix} \qquad (6)$$

With these definitions we can write the relationship between transmitted data bits and the outputs of the MC-AcR as an extended MIMO model

$$\mathbf{y} = \mathbf{H}(\mathbf{s} \odot \mathbf{s}) + \mathbf{G}(\mathbf{s} \,\tilde{\otimes}\, \mathbf{s}) + \boldsymbol{\nu} \qquad (7)$$

where the symbol $\odot$ denotes an element-wise multiplication, while $\tilde{\otimes}$ denotes a reduced Kronecker product that accounts for those combinations of values from $\mathbf{s}$ with unequal index. If we can guarantee that

$$h_{n,n'}^{[l]} = 0 \quad \forall\ n \neq n' \text{ and } \forall\ l \qquad (8)$$

which means that the filtered and unfiltered received subchannel pulses are orthogonal for every receiver channel, the interference matrix will vanish and a standard linear MIMO signal model (in s_n^2) remains. Note that due to the binary data symbols, $s_n^2 = s_n$ and standard methods [6] can be used to separate the multichannel data. Section IV discusses the design of pulse shapes $w_n(t)$ for which this orthogonality condition holds. However, as the condition is imposed on the *received* subchannel pulses $g_n(t)$, the orthogonality might be impaired by the multipath transmission and hardware imperfections in the receiver.

A combiner matrix $\mathbf{W}$ is used in the digital linear receiver backend to compute the decision variables $\mathbf{z} = \mathbf{W}\mathbf{y}$. The decision variable of the i-th channel can be expressed as

$$z_{i,\text{sum}} = \mathbf{w}_i^T \left[\mathbf{h}_i s_i^2 + \sum_{j \neq i} \mathbf{h}_j s_j^2 + \mathbf{G}(\mathbf{s} \,\tilde{\otimes}\, \mathbf{s}) + \boldsymbol{\nu} \right] \qquad (9)$$

$$= z_i + z_i^{[\mathbf{H}]} + z_i^{[\mathbf{G}]} + z_i^{[\nu]}. \qquad (10)$$

Equation (10) is a decomposition of $z_{i,\text{sum}}$ into the components resulting from the i-th symbol and interference caused by all but the i-th column of $\mathbf{H}$, as well as by the non-zero crosscorrelation between the subchannels. The last term includes all noise contributions.

III. Performance characterization

The bit-error-rate (BER) performance of the proposed receiver structure has been analyzed in [1], [2]. In this section we introduce alternative performance measures that provide additional insight in the receiver operation and the invertibility of the MIMO problem (7). Such measures support the search for optimal pulse shapes for the MC-AcR.

A. Channel conditioning and interference

The MIMO model in (7) corresponds to a system of L linear equations for the data vector $\mathbf{s}$. Hence it is obvious that we must have $L \geq N$ to allow for an inversion of this system. In this case, the condition number of the channel matrix $\mathbf{H}$, defined as the ratio of the largest singular value of $\mathbf{H}$ to the smallest, is an intuitive measure for the problem invertibility.

Based on the decomposition of the decision variables $\mathbf{z}$ in (10) we also define a signal-to-interference ratio (SIR) as:

$$\text{SIR}_{\mathbf{H}+\mathbf{G}}(z_i) = 10 \log E_{\mathbf{H},\mathbf{G}} \left\{ \frac{E_{\mathbf{s}}^2 \{|z_i|\}}{\text{var}_{\mathbf{s}} \left\{ |z_i^{[\mathbf{H}]} + z_i^{[\mathbf{G}]}| \right\}} \right\} \qquad (11)$$

where $E_{\mathbf{H},\mathbf{G}}\{\cdot\}$ denotes expectation w.r.t. the channel realizations and $E_{\mathbf{s}}\{\cdot\}$ w.r.t. the data. This SIR relates the useful energy in the i-th channel's decision variable to the linear interference from $\mathbf{H}$ and the nonlinear crossterms between channels with unequal indices expressed by $\mathbf{G}$. Only the linear part of the interference plays a role when $\mathbf{G} = \mathbf{0}$, and the resulting $\text{SIR}_{\mathbf{H}}$ can be understood as a "degree of orthogonalization" that is achieved by the backend processing.

If we consider the decomposition of the signal at the receiver output from (4) again, we note that whenever the orthogonality condition (8) does not hold, the corresponding $z_i^{[G]}$ will be non-zero. In this case, the number of interference crossterms scales with $N(N-1)$ while the number of useful signal-by-signal terms just scales with N and the SIR and BER performance will probably degrade.

To evaluate the energy capture of the MC-AcR, we also define a signal-to-noise ratio (SNR) for the decision variables

$$\text{SNR}(z_i) = 10 \log E_{\mathbf{H},\mathbf{G}} \left\{ \frac{E_{\mathbf{s}}^2 \{|z_i|\}}{\text{var} \left\{ |z_i^{[\nu]}| \right\}} \right\} \qquad (12)$$

B. Performance bound and interference cancellation

A fundamental bound for MIMO receivers is the so-called perfect interference cancellation (PIC) bound [6]. It can be obtained by multiplying the frontend output vector $\mathbf{y}$ with the so-called *matrix matched filter* $\mathbf{H}^*$, the Hermitian transpose of the channel matrix. This results in a vector $\tilde{\mathbf{y}}$

$$\tilde{\mathbf{y}} = \mathbf{H}^*\mathbf{H}\mathbf{s} + \mathbf{H}^*\nu \qquad (13)$$

The matrix $\mathbf{H}^*\mathbf{H}$ contains all the correlations of the columns of $\mathbf{H}$. A receiver that knows each interfering symbol $s_{j\neq i}$ for the desired symbol s_i can subtract all the linear interference terms mentioned in (10). It's decision variables can be expressed as

$$\mathbf{z}_{\mathrm{PIC}} = \mathrm{diag}\left\{\mathbf{H}^*\mathbf{H}\right\}\mathbf{s} + \mathbf{H}^*\nu. \tag{14}$$

This hypothetical receiver is used as a performance bound in BER simulations as it is neither impaired by linear interference from $\mathbf{H}$ nor by nonlinear interference from $\mathbf{G}$.

IV. Transmit signal generation

We use two different types of transmit signal subchannel pulses for the performance evaluation, an UWB-OFDM signal and subchannel pulses obtained by the genetic optimization algorithm. In general, both are multichannel impulse-radio (IR) schemes which use a set of ultra-short pulses for the $w_n(t)$. The pulses are modulated by the binary data symbols and extended with a zero guard interval (GI) to avoid ISI. This GI is chosen such that the overall symbol duration is 100 ns or 50 ns, depending on the simulation scenario. We use binary pulse-position-modulation to allow for a zero detection threshold at the receiver.

The performance simulations use an AcR where the filters $f_l(t)$ are pure delays from a set $\{D_l\}$. The spacing of these delays is chosen on the order of the inverse overall system bandwidth [2]. The integration interval is 23 ns for all schemes.

A. UWB OFDM signal

Like in the original proposal we use an OFDM signal consisting of a rather low number of subcarriers in order to allow for a larger subchannel bandwidth. In [1] it has been shown that a greater bandwidth has a beneficial influence on the transmission scheme in terms of fading resistance. A typical number of subchannels is $N = 9$, each one using a bandwidth of 500 MHz. The $w_n(t)$ for this scheme are sinusoidal subcarriers using a root-raised-cosine pulse for shaping their spectrum.

At the receiver side we typically use $L = N + 1$ channels to separate the subchannels. The individual receiver delay lags are on the order of one nanosecond and below, like in [2].

B. Pulses obtained by the genetic optimization algorithm

As a large signal bandwidth is desirable in terms of fading resistance, another set of pulses $w_n(t)$ should be found where each pulse uses the overall signal bandwidth, which was approximately 4 GHz. We use $L = N$ receiver channels to keep the complexity as low as possible. The approach is to find subchannel signals for which (8) holds, which in the case of a pure MC-AcR is the condition that the cross-correlation functions (CCF) of the received pulses vanish at the receiver delay lags. This can be formalized with a mean-square cross-correlation measure (see also [7] for variations) for the design of the i-th pulse

$$\mu_{\mathrm{ccf},i} := \sum_{j=1}^{i-1} \sum_{D_l \in \{D_l\}} |\Phi_{w_i w_j}(D_l)|^2 \tag{15}$$

where $\{D_l\}$ is the set of all AcR delay lags, $\Phi_{w_i w_j}(D_l)$ is the energy-normalized CCF of $w_i(t)$ and $w_j(t + D_l)$ and $\mu_{\mathrm{ccf},1} = 0$ per definition. The N subchannel pulses are designed sequentially.

As it can be seen from (5) and (6), the n-th column of the channel matrix corresponds to samples of the autocorrelation function (ACF) of the n-th subchannel's received pulse. We expect that the ACF is not influenced as severely by the multipath propagation as the pulse shape itself [5]. Hence we design the $w_n(t)$ in such a way that the i-th subchannel's ACF has a distinct peak at the delay of the i-th receiver channel. The height of this peak is again measured by a correlation measure

$$\mu_{\mathrm{acf},i} := \begin{cases} 1/2 - |\Phi_{w_i w_i}(D_i)| & \text{for } |\Phi_{w_i w_i}(D_i)| < 1/2 \\ 0 & \text{otherwise} \end{cases} \tag{16}$$

which saturates at zero for ACF values of $1/2$ and larger. Note that $\Phi_{w_i w_i}(D_i)$ is normalized such that $\Phi_{w_i w_i}(0) = 1$. To orthogonalize the columns of $\mathbf{H}$ we further aim at minimizing the i-th channel's ACF at all but the i-th delay lag used by the AcR. This can be done by minimizing the measure

$$\overline{\mu}_{\mathrm{acf},i} := \frac{1}{N-1} \sum_{D_l \in \{D_l\} \setminus D_i} |\Phi_{w_i w_i}(D_l)|^2 \tag{17}$$

We use the genetic algorithm [3] for the optimization of these correlation properties. The i-th pulse $w_i(t)$ is the one that minimizes the cost function $\mathcal{C}(w_i(t))$ assembled from the correlation measures introduced above

$$w_i(t) = \arg\min_{w_i(t)} \mathcal{C}(w_i(t)) = \mu_{ccf,i} + \mu_{acf,i} + \overline{\mu}_{acf,i} \tag{18}$$

We use sequences of a length of 200 samples in the optimization. The population of the GA is selected as 100 sequences that are randomly initialized. A key problem is that there exist fundamental bounds for the simultaneous optimization of ACF and CCF properties [8] of a set of signals, especially if the pulse-length is constrained like in IR-UWB.

V. Performance simulations and results

For the performance simulations, we use a transmitted signal as in (1), with the set $\{w_n(t)\}$ generated as explained in Section IV. Concerning the backend, we use an MMSE combiner [6] as well as a pre-defined DFT matrix for the OFDM scheme. The latter estimates the subcarrier energies in frequency domain [1]. The MMSE backend needs to estimate the channel matrix from training symbols, which is not the case for the DFT scheme. Multipath CIRs are generated using statistical channel models. We use three different scenarios as described in Table I.

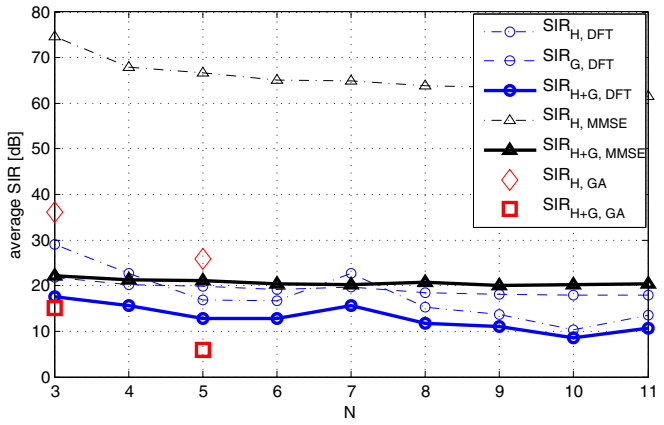

Fig. 2. Different contributions to the SIR for the DFT and MMSE backend and the OFDM scheme as a function of N as well as for two exemplary values of N for the GA scheme. For OFDM and MMSE, the $\mathrm{SIR}_{\mathbf{G}}$ dominates the total SIR and is not shown. Channel scenario II is used.

TABLE I
CHANNEL MODELS AND PARAMETERS USED IN SIMULATIONS

Parameter	Scenario		
	I	II	III
LOS/NLOS	LOS	NLOS	NLOS
RMS delay spread τ_{rms}	4 ns	8 ns	15 ns
Ricean K-factor	1	0	0
Symbol duration $\mathrm{T}_{\mathrm{sym}}$ (incl. GI)	100 ns	100 ns	50 ns

Fig. 2 shows simulation results for the SIR defined in (11) as a function of the number of subchannels N. The values for the SIR in the results are averaged over the decision variables. Considering only $\mathrm{SIR}_{\mathbf{H}}$, the MMSE backend clearly achieves a high amount of orthogonalization, which is not the case for the DFT scheme. The total SIR for MMSE is dominated by the $\mathrm{SIR}_{\mathbf{G}}$. For the GA scheme, the SIR decreases for $N = 5$ while for OFDM it is approximately constant over N. Therefore the OFDM scheme scales very well with N, which is also reflected in the BER results in Fig. 3.

The BER curve for the GA scheme at $N = 5$ shows an error floor, while for OFDM it drops steeply, even for $N = 9$. In general, the frequency separation of the OFDM subcarriers allows for the orthogonality condition (8) to hold, even for larger values of N. For the GA scheme, the ACF and CCF properties of the $\{w_n(t)\}$ can not be optimized arbitrarily as mentioned in Section IV-B. A hypothetical BER with $\mathbf{G} = \mathbf{0}$ is shown for the GA scheme with $N = 5$. Here the performance is quite close to the corresponding PIC bound, which indicates that the nonlinear interference is the main impairment. For OFDM, the interference from $\mathbf{G}$ causes only a negligible impairment, which is confirmed by the fact that the its performance for the MMSE backend is very close to the PIC bound. This indicates very low crosscorrelation between the channels as well as very low linear interference.

Until now we have assumed an ideal synchronization of the receiver, i.e. $\tau_0 = 0$ in (2). To account for an important practical situation, also non-zero values for τ_0 are evaluated. Fig. 4 shows an example for one noise-free symbol using channel scenario I and an ideal integration window as well as one with $\tau_0 = 3\mathrm{ns}$. We expect that especially for LOS scenarios,

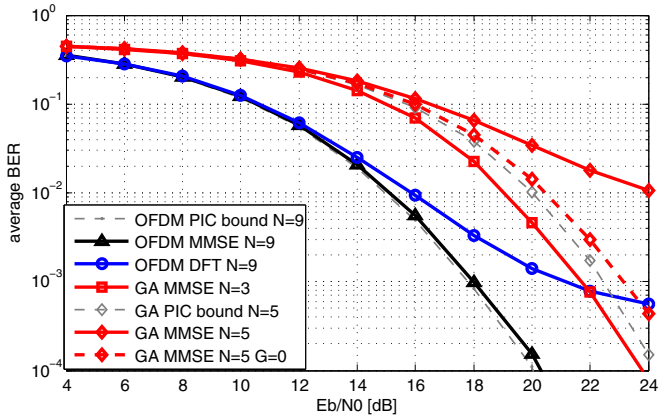

Fig. 3. BER for DFT and MMSE backends using the OFDM scheme with $N = 9$ and channel scenario II, as well as the genetically optimized scheme (GA) with $N = 3$ and $N = 5$, and scenario I. Also shown is the hypothetical BER of the GA scheme for $N = 5$ if the interference matrix $\mathbf{G} = \mathbf{0}$.

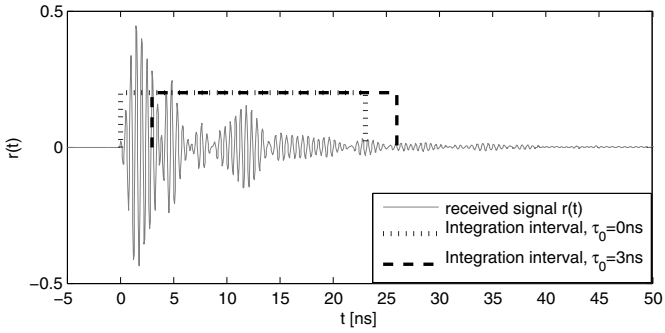

Fig. 4. One symbol without noise together with the integration window with $T_I = 23\mathrm{ns}$ for channel scenario I. The dotted line corresponds to an ideal integration start, the dashed line to an offset of +3 ns.

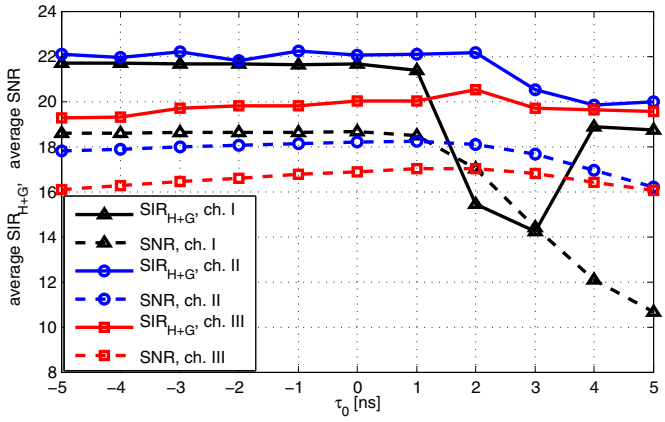

Fig. 5. SIR and output SNR for OFDM with $N = 9$ and MMSE backend as a function of integration window start offset τ_0 for channels I (triangle markers), II (circle markers) and III (square markers).

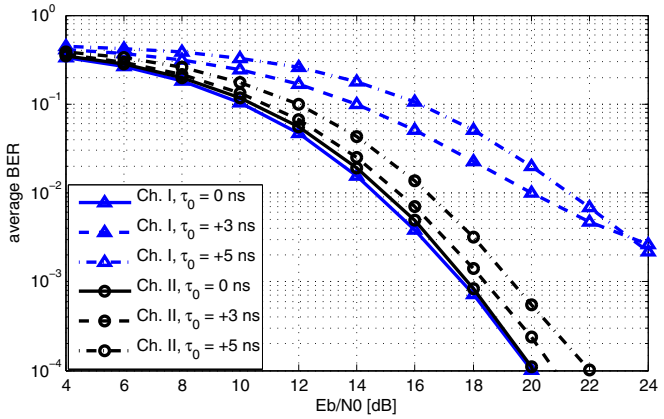

Fig. 6. BER for the MMSE backend using the OFDM scheme with $N = 9$ for channel scenarios I (triangle markers) and II (circle markers) and offsets τ_0 of 0, 3 and 5 ns.

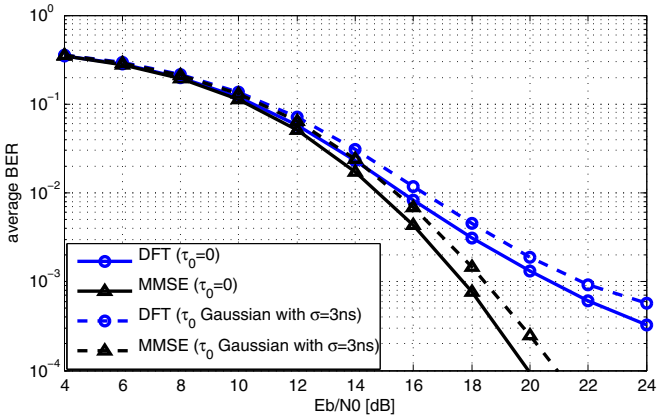

Fig. 7. BER for the DFT and MMSE backends using the OFDM scheme with $N = 9$ for the channel scenario II. The solid curves show the BER with an ideal synchronization, the dashed lines use a Gaussian synchronization offset with mean equal to the ideal $\tau_0 = 0$ and a standard deviation of 3ns.

a large positive offset of τ_0 leads to a performance penalty as much of the energy of the symbol is lost. In general, as the main signal component is not within the integration period, the orthogonality condition (8) will be violated. Therefore, both linear and nonlinear interference terms will increase.

This is confirmed by Fig. 5, which shows the $\mathrm{SIR}_{\mathbf{H+G}}$ and SNR for channel scenarios I, II and III. Concerning the SIR, we indeed observe a degradation for the LOS channel, especially for an offset of +3 ns. Although the $\mathrm{SIR}_{\mathbf{H+G}}$ increases again for larger values of τ_0, this is only due to the nonlinear contribution $\mathrm{SIR}_{\mathbf{G}}$, the linear part $\mathrm{SIR}_{\mathbf{H}}$ decreases monotonically for $\tau_0 > 0$. For clarity, only the total SIR is shown. The output SNR decreases, as less energy can be captured. For the longer NLOS channels, both the SIR and SNR are far more robust to a synchronization offset, as the symbol energy is spread out over a longer duration and the linear transmission effects cause no significant loss of orthogonality. For scenario III, there is slight ISI, which causes the $\mathrm{SIR}_{\mathbf{H}}$ to degrade and causes an overall loss of the total SIR. The channel matrix condition numbers for all scenarios are between 3.8 and 5.2, indicating a good invertibility.

The effects of the synchronization offset on the BER for $N = 9$ and the MMSE backend are illustrated in Fig. 6. For the NLOS channel, the performance degradation is not severe, even for a large error of 5 ns. The effect is more pronounced for the short LOS channel, where a positive offset causes a considerable loss of energy capture. Interestingly, for high E_b/N_0, we observe that the BER is lower for $\tau_0 = 5$ than for $\tau_0 = 3$. Comparing with Fig. 5, we conclude that the considerable drop in the SIR at $\tau_0 = 3$ leads to an error floor in the BER, which is not the case for the larger offset where the SIR is higher.

Fig. 7 shows the BER performance over channel scenario II where τ_0 is drawn from a Normal distribution with zero mean and a standard deviation of 3 ns. We observe that both MMSE and DFT backend are not severely degraded although the choice of the distribution for τ_0 allows for large synchronization errors.

VI. Conclusion

We have investigated a robust, noncoherent UWB receiver that is able to separate a high-rate multichannel signal at low complexity. A UWB OFDM signal seems best suited as transmit signal. It clearly outperforms a scheme that uses spread-spectrum sequences with optimized correlation properties and its data rate scales without performance penalty. A practical MMSE backend is used, with a frontend consisting of a multichannel autocorrelation receiver.

Several performance measures have been introduced and discussed, which shed light on the influence of imperfections in the transmission chain. Synchronization offset has been considered as an example. The evaluated performance measures confirm the robustness of the proposed transceiver. Further work will include the evaluation of imperfections in the frontend delay filters and RF mixers.

References

[1] K. Witrisal, "Noncoherent autocorrelation detection of orthogonal multicarrier UWB signals," in *IEEE Intern. Conf. on Ultra-Wideband, ICUWB*, Hannover, Germany, Sep. 2008, invited paper.

[2] ——, "A noncoherent multiband receiver for IEEE802.15.4a UWB signals," in *COST 2100 Managem. Comm. Meeting*, Trondheim, Norway, Jun. 2008, COST 2100 TD(08)545.

[3] J. H. Holland, *Adaption in Natural and Artificial Systems*. Ann Arbor: University of Michigan Press, 1975.

[4] F. Nekoogar and F. Dowla, "Performance of multiple pulse multiple delay modulated UWB signals in a multiple access indoor wireless channel," in *IEEE Pacific Rim Conf. on Commun., Computers and Signal Proc., PACRIM*, vol. 2, Aug. 2003, pp. 545–548.

[5] K. Witrisal and M. Pausini, "Statistical analysis of UWB channel correlation functions," *IEEE Trans. Veh. Technol.*, vol. 57, no. 3, pp. 1359–1373, May 2008.

[6] J. R. Barry, E. A. Lee, and D. G. Messerschmitt, *Digital Communication*, 3rd ed. Boston, USA: Kluwer, 2004.

[7] H. Donelan and T. O'Farrell, "A new Method for generating Sets of Orthogonal Sequences for a Synchronous CDMA System," *Lecture Notes in Computer Science, Springer Berlin / Heidelberg*, vol. 1746/1999, p. 799, 1999.

[8] D. Sarwate and M. B. Pursley, "Crosscorrelation properties of pseudorandom and related sequences," *Proceedings of the IEEE*, vol. 68, no. 5, pp. 593–619, May 1980.